

High-aspect ratio titanium nanopillars modulate macrophage responses

Eijkel, Benedictus I.M.; Modaresifar, Khashayar; Má dai, Eszter; Ganjian, Mahya; Taheri, Peyman; Apachitei, Iulian; Fratila-Apachitei, Lidy E.

DOI

[10.1016/j.bioadv.2025.214321](https://doi.org/10.1016/j.bioadv.2025.214321)

Publication date

2025

Document Version

Final published version

Published in

Biomaterials Advances

Citation (APA)

Eijkel, B. I. M., Modaresifar, K., Má dai, E., Ganjian, M., Taheri, P., Apachitei, I., & Fratila-Apachitei, L. E. (2025). High-aspect ratio titanium nanopillars modulate macrophage responses. *Biomaterials Advances*, 175, Article 214321. <https://doi.org/10.1016/j.bioadv.2025.214321>

Important note

To cite this publication, please use the final published version (if applicable).
Please check the document version above.

Copyright

Other than for strictly personal use, it is not permitted to download, forward or distribute the text or part of it, without the consent of the author(s) and/or copyright holder(s), unless the work is under an open content license such as Creative Commons.

Takedown policy

Please contact us and provide details if you believe this document breaches copyrights.
We will remove access to the work immediately and investigate your claim.



High-aspect ratio titanium nanopillars modulate macrophage responses

Benedictus I.M. Eijkel^{a,*}, Khashayar Modaresifar^a, Eszter Mádai^b, Mahya Ganjian^a,
Peyman Taheri^b, Iulian Apachitei^a, Lidy E. Fratila-Apachitei^{a,*}

^a Department of Biomechanical Engineering, Faculty of Mechanical Engineering, Delft University of Technology (TU Delft), Mekelweg 2, 2628 CD Delft, the Netherlands

^b Department of Materials Science and Engineering, Faculty of Mechanical Engineering, Delft University of Technology (TU Delft), Mekelweg 2, 2628 CD Delft, the Netherlands

ARTICLE INFO

Keywords:

Dry-etched titanium
Black titanium
ICP-RIE
Macrophages
Immunomodulation

ABSTRACT

Titanium surfaces featuring high-aspect ratio (HAR) nanopillars can have antimicrobial and osteogenic properties. Nevertheless, the impact of these surfaces on immune cells and their potential for immunomodulation remain unclear. In this study, the effects of HAR titanium nanopillars produced by dry-etching (DETi) on the response of unstimulated (M0) and pro-inflammatory (M1) murine macrophages (J774A.1) have been explored. The findings revealed changes in the morphology and crystallinity of the DETi nanopillars along their height. After 48 h of culture, both M0 and M1 stimulated macrophages displayed a more elongated morphology, a smoother cell surface, and shorter cellular protrusions on the more hydrophilic and rough DETi surfaces. Furthermore, DETi surfaces induced polarization of M0 cells towards M2 phenotypes, whereas M1 stimulated cells showed M2-like elongated morphologies while maintaining a stronger pro-inflammatory response to DETi surfaces relative to the glass control. The findings indicate that the DETi surfaces can induce morphological changes in macrophages and specific immunomodulatory effects depending on their initial phenotype, highlighting the potential of such biomaterials to incorporate an immunomodulatory biofunctionality next to the osteogenic and bactericidal ones.

1. Introduction

Titanium-based biomaterials featuring specific surface topographies have a strong potential to modulate cellular responses for bone implants [1,2]. In particular, high-aspect ratio (HAR) titanium nanopillars represent promising topographies in the fight against implant-associated infections (IAI) and antimicrobial resistance (AMR). This is due to their bactericidal properties based on contact-killing mechanisms, with no documented evidence of bacteria developing resistance to such titanium surfaces [3–5]. Importantly, these surfaces exhibit not only bactericidal properties [6,7] but also impart other cell instructive properties for mammalian cells through their nanoscale features [2,8,9], potentially induced through mechanotransduction pathways [10]. Consequently, they are also referred to as biological metamaterials [4].

Multiple methods can be used to fabricate titanium-based HAR structures, including wet-etching (*i.e.*, hydrothermal etching) [11–13] and dry-etching [8,9,14]. While wet etching is simpler and more cost-effective than dry-etching methods, it is not without drawbacks, including limited control of pattern features, resulting in randomly

oriented nanowires instead of nanopillars, and long etching times (a few hours compared to a few minutes with dry-etching) [15]. These limitations constrain precision and the maximum achievable aspect ratio, thereby limiting the optimization of the target biofunctionality. Dry-etching (*i.e.*, reactive ion etching, RIE) accelerates ions towards the substrate to etch away the surface. While regular RIE tends to be highly isotropic, like wet-etching, inductively coupled plasma RIE (ICP-RIE) introduces a significant enhancement. In ICP-RIE, atoms are propelled at high-velocity perpendicular to the material surface, resulting in a highly anisotropic process [7,14]. This contributes to increased control of pattern features, etching selectivity, and reproducibility compared to wet-etching methods. Although the process requires dedicated and more expensive equipment, and optimization of multiple conditions to obtain the desired pattern on titanium surfaces, such as chamber temperature, gas inflow, and pressure [14,15], it offers superior capability compared to wet-etching and to other multiple-step patterning processes for generating HAR pillars on titanium with controllable features in a relatively short time. As a consequence, although initially used to create bactericidal HAR on silicon substrates [16,17], more recently, the ICP-

* Corresponding authors.

E-mail addresses: B.I.M.Eijkel@tudelft.nl (B.I.M. Eijkel), E.L.Fratila-Apachitei@tudelft.nl (L.E. Fratila-Apachitei).

<https://doi.org/10.1016/j.bioadv.2025.214321>

Received 17 February 2025; Received in revised form 15 April 2025; Accepted 22 April 2025

Available online 23 April 2025

2772-9508/© 2025 The Authors. Published by Elsevier B.V. This is an open access article under the CC BY license (<http://creativecommons.org/licenses/by/4.0/>).

RIE process has started to be explored for fabricating HAR titanium pillars, also referred to as black titanium (bTi) [2,6,10], maskless dry etching [15] or ICP-RIE titanium [14].

Hitherto, the effects of these dry-etched titanium surfaces (DETi) on the response of immune cells have not been investigated. These effects strongly influence peri-implant bone regeneration and long-term implant survival [18]. The initial pro-inflammatory response following implantation is needed for clearing the tissue site of cell debris and pathogens, and signaling the tissue repair cells, such as mesenchymal stromal cells (MSCs), to enable tissue regeneration and implant osseointegration. This interplay between immune and osteoprogenitor cells, termed osteoimmunology, relies on a fine balance between the pro- and anti-inflammatory response of macrophages that is also influenced, and possibly mediated, by the biomaterials characteristics [19].

In addition to the critical role in osteoimmunomodulation, macrophages also play a crucial part in preventing implant failure attributed to IAI by eliminating bacteria from the implant surface. Enhancing the body's capacity for bacterial clearance, in addition to the biomaterial's inherent bactericidal properties, can reduce IAI-related implant failure rates while enhancing osseointegration [20]. This involves a comprehensive understanding of both pro- and anti-inflammatory responses of macrophages to a biomaterial and the role these responses may play in combating bacteria and improving osteogenesis.

To unravel the possible immunomodulatory potential of DETi, the present study investigated the effects of DETi on unstimulated (M0) and pro-inflammatory (M1) macrophages. Following a multiscale physico-chemical characterization of the DETi substrates, the temporal changes in cell morphology and gene profiles have been assessed and discussed in relation to the properties of the DETi surfaces.

2. Materials and methods

2.1. Fabrication of dry-etched titanium samples

The titanium samples were dry-etched using ICP-RIE equipment (PlasmaLab System 100, Oxford Instruments, UK) following a previously established protocol [9,14] (Fig. 1a). Firstly, high-purity annealed titanium wafers (99.6 %, 100 mm in diameter, 125 μm thickness, Grade 2 - ASTM B265, Goodfellow, UK) underwent chemical-mechanical polishing (CMP Mecapol E460, France). The polishing process was performed with a slurry containing 25 % silicate (SiO_2) particles, 75 % demi water (dH_2O), and < 1 % potassium hydroxide (KOH). Polishing of the wafer consisted of 4 steps. First, the polishing head landed on the wafer with a working pressure of 0.40 bar for 10 s; following this, polishing was initiated at 1.50 bar for 120 s, followed by two rinsing steps of 0.80 bar for 10 s, and 0.40 bar for 60 s. Next, the wafer was rinsed with dH_2O , and after conditioning the machine, the polishing was repeated for 20 cycles. Following a photoresist coating to safeguard the surface, the polished titanium (pTi) wafers were then precision-cut to fit inside a 48-well plate ($8 \times 8 \text{ mm}^2$) by using a Disco dicer (Disco Hi-Tec Europe GmbH, Germany). Next, the pTi samples were cleaned through sequential immersions in acetone, ethanol, and isopropanol for 15 min each, followed by a spin-drying process. Before etching, the samples were mounted on a 4-in. fused SiO_2 carrier wafer backed with an aluminum layer (Fig. 1a); a thermal joint compound (type 120, Wakefield Engineering, USA) was applied in between the samples and the carrier wafer to enhance thermal conductivity. Before dry-etching, the ICP-RIE chamber was cleaned of any residue by 10 min of pre-cleaning with SF_6 to ensure uniformity between different batches [15]. The samples were etched using Cl_2 and Ar gases (30 sccm/2.5 sccm) under the following conditions: an ICP power of 600 W, an RF power of 100 W, a chamber pressure set at 0.02 mbar, a temperature of 40 $^\circ\text{C}$, and total etching time of 10 min. Finally, the samples were detached from the carrier wafer and subjected to another round of thorough cleaning in acetone, ethanol, and isopropanol for 15 min each, followed by spin drying.

2.1.1. Physico-chemical characterization of dry-etched titanium

Within 48 h after fabrication and cleaning, a comprehensive analysis of both polished (pTi) and dry-etched titanium (DETi) surfaces was conducted, which included the morphology (surface and cross-section), chemistry (surface and cross-section), and wettability (Fig. 1b).

The surface morphology of the samples was examined by scanning electron microscopy (SEM; HELIOS NanoLab 650, FEI, USA) at 5 kV and 0.1 nA. For each batch, top and tilted (30°) images were acquired at different magnifications (1500 \times , and 5000 \times) to verify the uniformity and reproducibility of the surfaces. The surfaces were further characterized by measuring the average pore width (PW), pore length (PL), and ridge width (RW). For these measurements, the free software ImageJ (<https://imagej.net/software/fiji/downloads>) was utilized. At least three samples were used for these measurements, with five separate SEM images taken of each sample from different areas of the surface. The reported values represent the mean and standard deviation.

The surface roughness (S_a) of both pTi and DETi samples was obtained with a Profilom3D optical profilometer (Filmetrics, USA) to capture the representative morphological features of the surfaces. The 3D profiles were acquired using white light interferometry, a 50 x objective, and the envelope peak model. Post-processing of the images was required to filter out outliers; thereafter, a 3×3 minimum filter was applied to smoothen out the features, and finally, all invalid data points were calculated by interpolation of neighboring pixels. Five samples were used for each group, and for each, 3D profiles were taken from four separate areas of the surface. An average value was calculated based on these measurements. The reported values represent the mean and standard deviation.

The pTi and DETi wettability parameters were identified using static contact angle measurements by a drop-shape analyzer (DSA 100, Kruss, Germany). Images were captured 0.1 s after 0.5 μL deionized water was released from the needle tip. The fitting methods used for pTi and DETi were Young Laplace and Circle, respectively. For each group, at least three separate samples were used to acquire the water contact angle. The data is represented as an average value with a standard deviation.

The cross-section analysis of DETi samples was performed by transmission electron microscopy (TEM, FEI cubed Cs corrected Titan, USA). In scanning mode (STEM), Annular Dark Field (ADF) images and Selected Area Diffraction Patterns (SADP) were collected. From these images, the pillar height (PH) was estimated. Energy Dispersive X-ray (EDX) spectra were collected for each beam position in a STEM image for elemental mapping using the super-X detector in the ChemiSTEMTM configuration. High-resolution STEM lattice images were collected on a Thermo Scientific CetaTM 16 M.

In addition, the phase composition of the samples was investigated using a 2D X-ray diffractometer (XRD, D8 Discover diffractometer, Bruker, Germany) fitted with a Cu K_α source at 50 kV and 1000 μA , in the range $2\theta = 10^\circ - 110^\circ$ at a step size of $0.040^\circ 2\theta$. The identification process was guided by the ICDD pdf4 database.

Finally, X-ray photoelectron spectroscopy (XPS) spectra were acquired by utilizing non-monochromatic Al K α radiation produced from an X-ray source featuring an Al anode, operating at 200 W and 13.1 kV. The primary photoelectron peaks for each element were captured with a step size of 0.1 eV and a measurement time of 1.25 s. This was achieved using a spherical capacitor analyzer configured with a pass energy of 71.55 eV. Photoelectrons were collected at take-off angles of 45° relative to the sample surface, approximately equivalent to a depth of 10 atomic layers, considering an inelastic mean free path of approximately 10×10^{15} \AA .

2.2. Macrophage culture

2.2.1. Pre-culture

The mouse macrophages (J774A.1, passage 12-14, Merck KGaA, Germany) were cultured in T75 flasks using Dulbecco's Modified Eagle Medium (DMEM, Thermo Fisher Scientific, USA) supplemented with 10

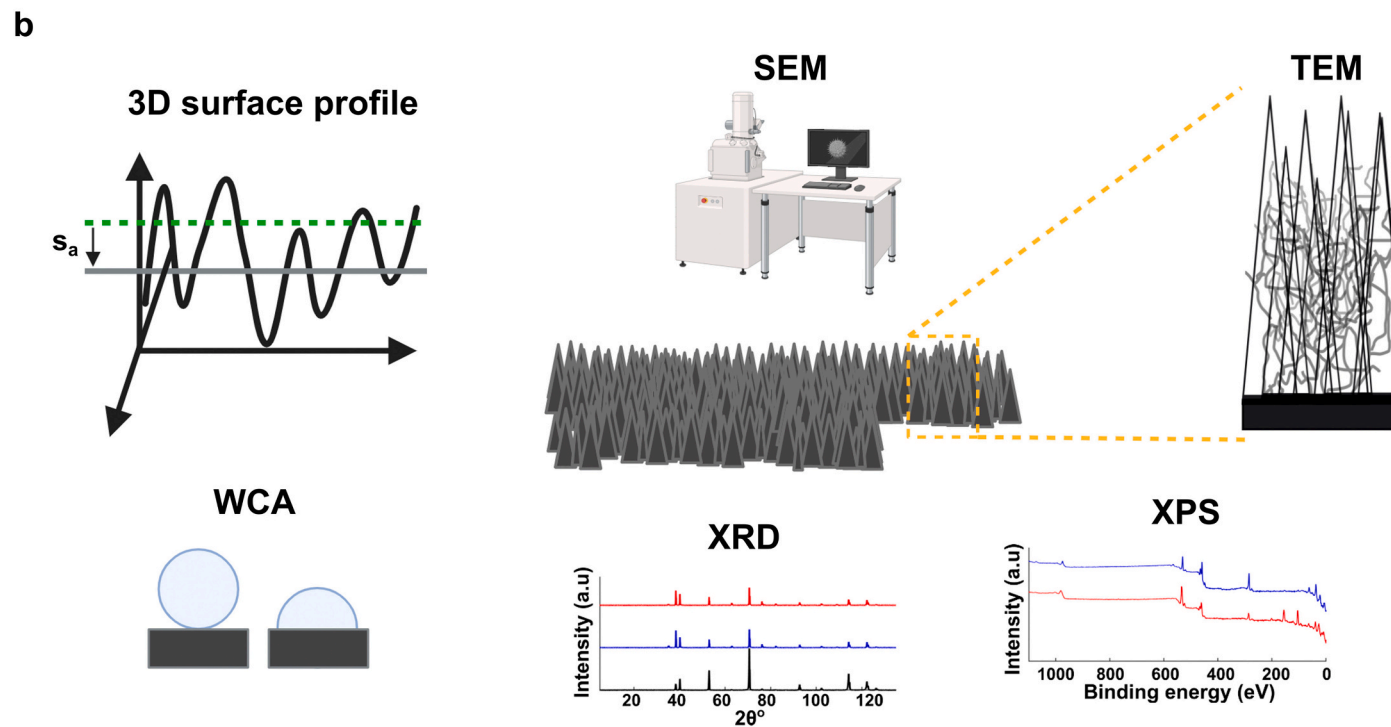
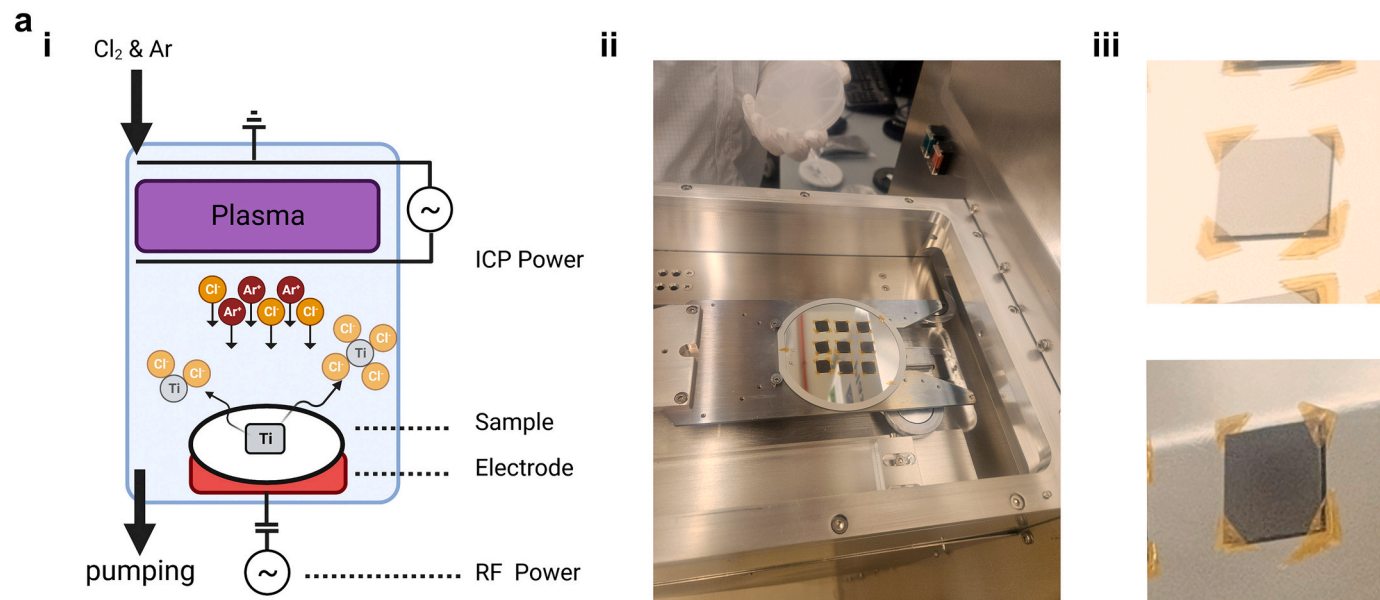


Fig. 1. a) i) Graphical representation of inductively coupled plasma reactive ion etching (ICP-RIE) using Cl and Ar ions (biorender.com); ii) image of the titanium samples in the loading chamber of the ICP-RIE; iii) polished titanium before (top) and after ICP-RIE (bottom); b) overview of physicochemical characterization methods. Clockwise from top-left: 3D surface profile measurements; scanning electron microscope (SEM); cross-sectional transmission electron microscopy; X-ray photoelectron spectroscopy (XPS); X-ray diffraction analysis (XRD); and water contact angle (WCA) measurements (biorender.com).

% (v/v) fetal bovine serum (FBS, Thermo Fisher Scientific, USA) and 1 % penicillin-streptomycin (Thermo Fisher Scientific, USA) at 37 °C and 5 % CO₂. Culture medium was refreshed every 2-3 days until the cells reached confluence. When the cells reached 80 % confluence, they were detached from the pre-culture flasks, using a cell scraper, counted, and seeded.

2.2.2. Cell seeding

Before each cell culture experiment, the pTi and DETi samples were sterilized with 70 % ethanol. The samples were then washed twice with Dulbecco's phosphate-buffered saline (PBS) followed by UV-light exposure for 20 min, and placed inside a 48-well plate (Greiner, Bio-One, Netherlands). Glass coverslips were used as control surfaces (Ctrl). Before seeding, the samples were incubated in a culture medium at 37 °C and 5 % CO₂ for at least 30 min to allow for protein adsorption. Macrophages were seeded at a density of 15,000 cells/cm² for the short-term experiments (two days), and at a density of 5000 cells/cm² for the long-term experiments (seven days). M1 polarization of macrophages was performed by the addition of 100 ng/mL Interferon- γ (IFN- γ , Sigma-Aldrich, Germany) and 10 ng/mL Lipopolysaccharide (LPS, Sigma-Aldrich, Germany) into the DMEM medium. Unstimulated macrophages were referred to as M0.

2.2.3. qPCR

The gene expression of M0 and M1 macrophages cultured on the pTi, DETi and Ctrl samples was assessed at 4, 24, and 48 h. The pro-inflammatory markers included tumor necrosis factor α (*TNF α*), interleukin-1 β (*IL1 β*), nuclear factor κ B (*NF κ B*), interleukin-6 (*IL6*), and a cluster of differentiation 86 (*CD86*). The anti-inflammatory markers were interleukin-10 (*IL10*), bone morphogenetic protein-2 (*BMP2*), and mannose receptor (cluster of differentiation 206, *CD206*). Ubiquitin C (*UBC*) was chosen as the housekeeping gene. The primers of each gene are listed in more detail in Supplementary Table S1. In short, ribonucleic acid (RNA) was isolated for each time point using the RNeasy micro kit (Qiagen, Netherlands). RNA was then converted to cDNA using the Quantitect Reverse Transcription Kit (Qiagen, Netherlands). QPCR was performed, with 1.5 ng cDNA, on the Rotor X gene PCR, (Qiagen, Netherlands) using the Quantinova SYBR Green PCR Kit (Qiagen, Netherlands). The gene expression relative to *UBC* was determined by the Δ Ct method, where Gene Expression = $2^{-\Delta\text{Ct}}$, and $\Delta\text{Ct} = \text{Ct}_{\text{sample}} - \text{Ct}_{\text{UBC}}$. In total, 6 samples were assessed per condition based on two independent experiments.

2.2.4. ELISA

The cytokine presence in the supernatant was checked 2 and 7 days after seeding, using the Simple Step ELISA kits from Abcam for TNF- α and IL-10. After the supernatant was collected, it was centrifuged at 2000g for 10 min at 4 °C to remove cell debris and stored at -80 °C until processing. After subtraction of the blank wells, which contained only culture medium, a standard curve was created using the protocols provided, the OD for IL10 was measured at 450 nm and for TNF- α the fluorescence was read at 530 nm_{exc}/590 nm_{ems}, using a Victor X3 plate reader (PerkinElmer, The Netherlands). The protein concentrations were obtained by using the standard curve. For each condition, 3 replicates were analysed in duplo.

2.2.5. Cell morphology

The morphological changes of J774A.1 cells cultured on the pTi and DETi surfaces were observed using SEM (Helios NanoLab 650, FEI, USA) at 4, 24, and 48 h. In short, after washing the samples twice with PBS, the cells were fixed with 4 % (v/v) formaldehyde solution (Sigma-Aldrich, Germany) for 10 min at room temperature. The samples were then washed twice again with PBS and stored in PBS at 4 °C until the dehydration steps were performed. Dehydration of the samples was performed by firstly washing the samples twice with dH₂O for 5 min, followed by sequential immersion in a series of ethanol solutions (*i.e.*,

50 %, 70 %, and 96 % for 15, 20, and 20 min, respectively), air-dried overnight, and gold-sputtered before SEM imaging. At least 5 images per sample, with 9 samples from three independent experiments, were processed at 1000 \times magnification. Image processing was performed using the open-source software FIJI (<https://imagej.net/software/fiji/downloads>). In short, after the usage of the smoothen function, the threshold was set manually to convert the outline of the cells into a mask. Thereafter, the 'analyse particles' function was used to measure the change in cell area and cell aspect ratio, AR = Maximum Edge Length / Minimum Edge Length, over time. At least 50 randomly selected cells from different replicate samples were used for each condition.

The interface between the M1 cells and DETi surfaces was imaged in cross-section by focused ion beam-SEM (FIB-SEM, Helios G4 CX, FEI, USA). The samples were tilted to 52°, and the selected surfaces were milled using Gallium ions with a 6.5 pA ion beam to roughly mill the surface followed by a 1.1 nA ion beam to polish the last parts (Z = 1.2 μ m, operating voltage = 30 kV).

2.2.6. Metabolic activity of the cells

The PrestoBlue assay was used to assess the metabolic activity of both M0 and M1 macrophages on DETi, pTi, and Ctrl surfaces. After 4, 24, and 48 h of culture, the medium was replaced with 200 μ L fresh culture medium and 10 % Presto Blue reagent (Thermo Fisher Scientific, USA). Wells without cells and samples were filled with fresh culture medium and 10 % PrestoBlue reagent as the negative control. All samples were incubated for 1 h at 37 °C and 5 % CO₂. After incubation, 100 μ L of the Presto Blue solution from each well was transferred in duplo to a new well in a 96-well plate. Fluorescence was then read at a wavelength of 530 nm_{exc}/590 nm_{ems}, using a Victor X3 plate reader (PerkinElmer, The Netherlands). For each condition, 6 replicates were analysed. The average metabolic activity of the cells is reported after subtraction of the background fluorescence from the negative control without cells.

2.3. Statistical analysis

After confirmation of normality by the Shapiro-Wilks normality test in Prism (GraphPad Prism version 8.0.1 for Windows, GraphPad Software, USA, www.graphpad.com), unpaired *t*-tests with Welch's correction were used. Non-parametric Kruskal-Wallis with post-hoc Dunn's test to look for significance was performed for non-normally distributed data, as was the case for cell area and cell aspect ratio measurements. A two-way ANOVA was used to analyse the significance of the Presto Blue measurements over time, and a one-way ANOVA was used to determine the significance of the $2^{-\Delta\text{Ct}}$ values at each time point. Followed by Tuckey's multiple comparison tests to look for significance. All the values are presented as mean \pm standard deviation and a *p*-value below 0.05 was considered to indicate statistical significance.

3. Results

3.1. DETi characteristics

Following the ICP-RIE process applied under the selected conditions, the DETi surfaces revealed numerous stochastically distributed and clustered pillars that also highlighted the grain boundaries of the Ti substrate (Fig. 2a). The clustered pillars generated a network of irregular pores and ridges over the entire surface (Fig. 2b, c). The pores' width (PW) ranged between 50 nm and 2100 nm, and the pore length (PL) ranged between 50 nm and 4740 nm. The width of the ridges (RW) was approximately 157 \pm 78 nm. This topography resulted in an average surface roughness (*S_a*) of 259 \pm 50 nm compared to only 4 \pm 1 nm of the polished surfaces (pTi) (Fig. 2d, e). The DETi were highly hydrophilic with water contact angle (WCA) values of 11 \pm 4° compared to 66 \pm 14° in the case of pTi surfaces (Fig. 2f).

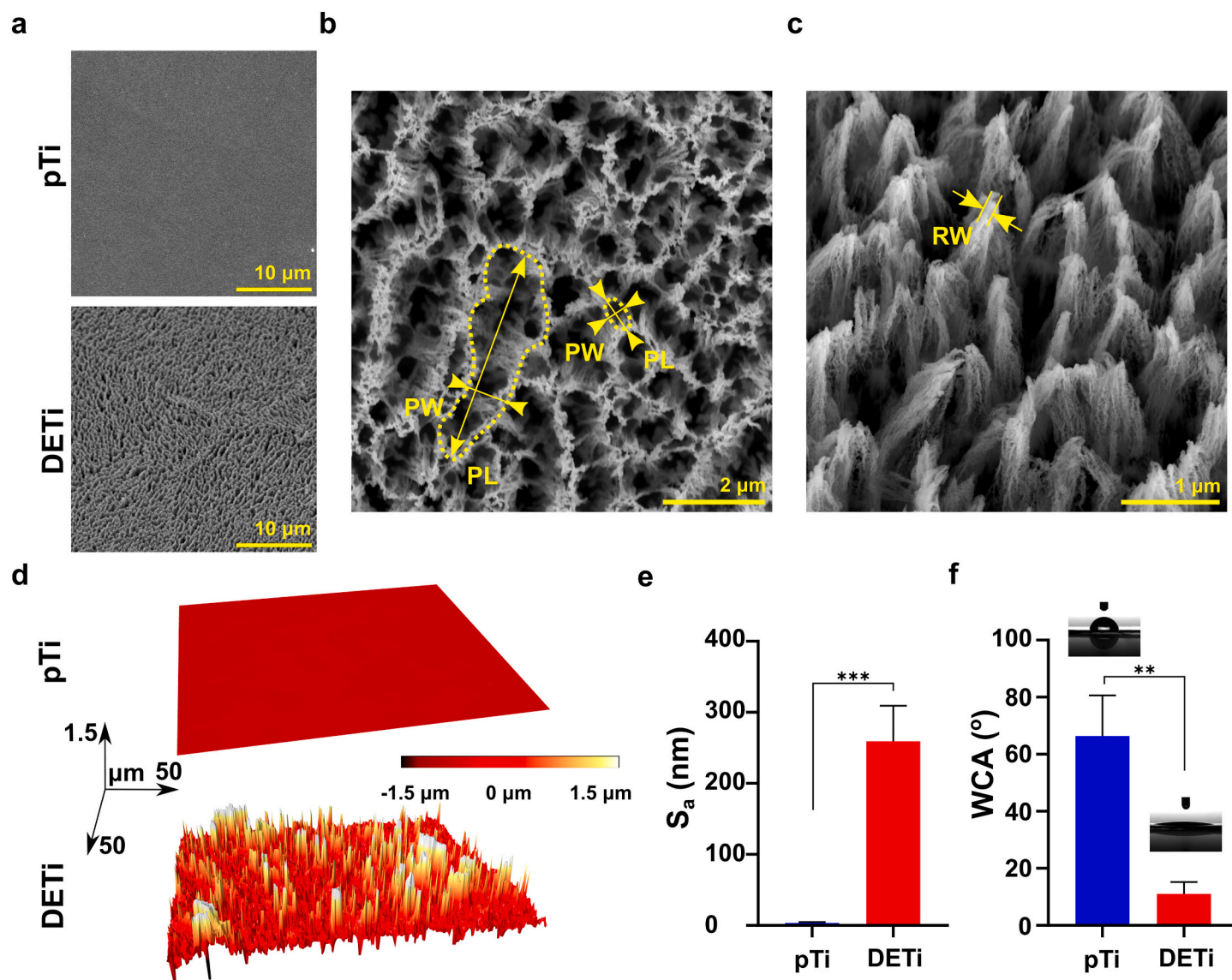


Fig. 2. a) SEM images of polished titanium (pTi) and dry-etched titanium (DETi) surfaces; b) top-view SEM of DETi with yellow lines and arrows indicating the pore width (PW) and pore length (PL); c) SEM image (30° tilt) of DETi showing the measured ridge width (RW); d) 3D profiles of pTi and DETi surfaces; e) average surface roughness (S_a) of pTi and DETi; f) water contact angle (WCA) for pTi and DETi surfaces. ** $p < 0.01$, *** $p < 0.001$.

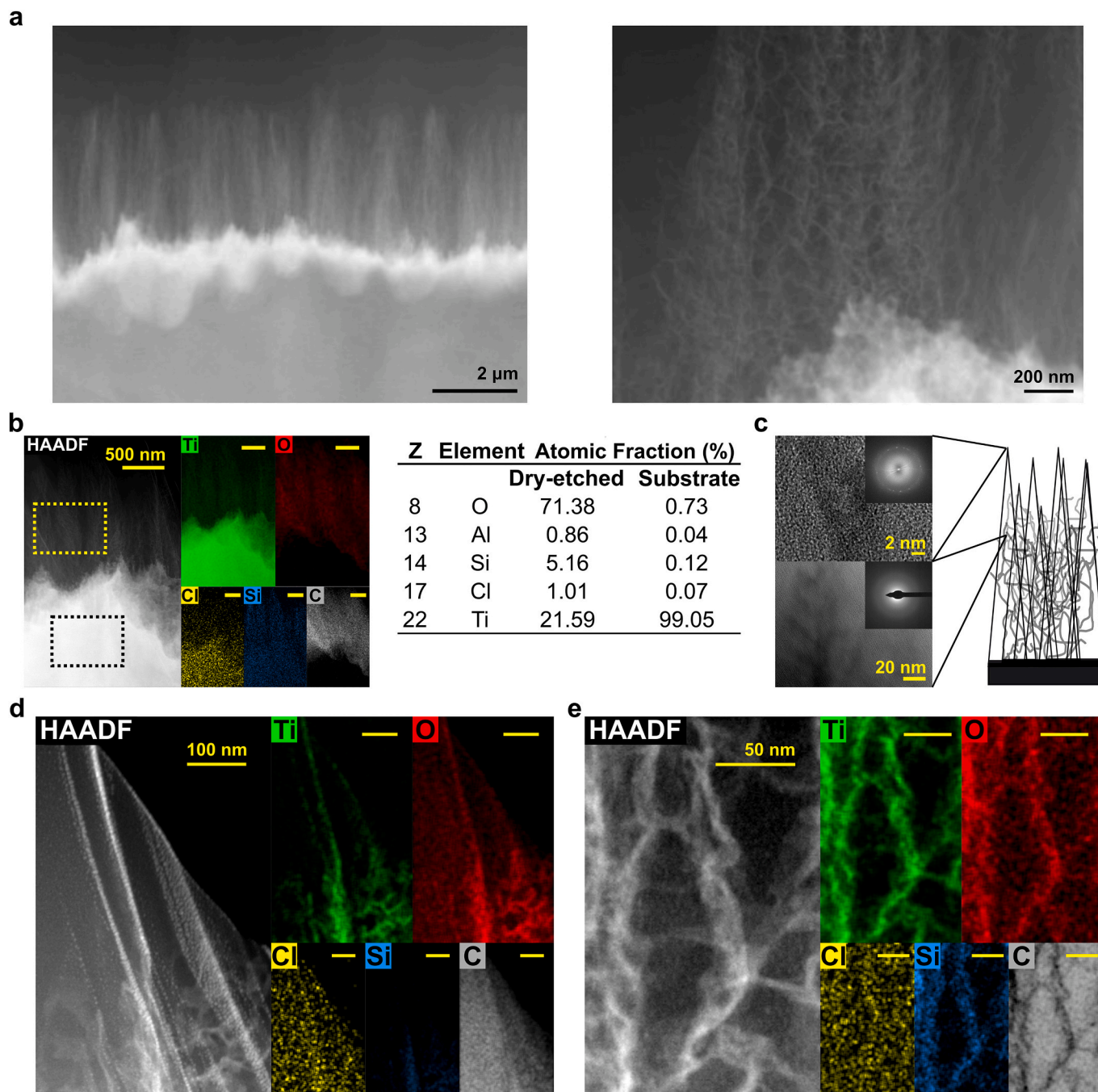


Fig. 3. a) High-angle annular dark-field (HAADF) cross-section scanning transmission electron microscope (STEM) images of dry-etched titanium (DETi) samples at two different magnifications; b) HAADF image and EDX elemental mapping of the DETi cross-sections; the table includes the elemental analysis of the dry-etched layer and the underlying Ti substrate; c) TEM-SADP images of the top and dendritic areas of the dry-etched layer; d) HAADF images and EDX elemental mapping of the top and e) dendritic areas of the dry-etched layer.

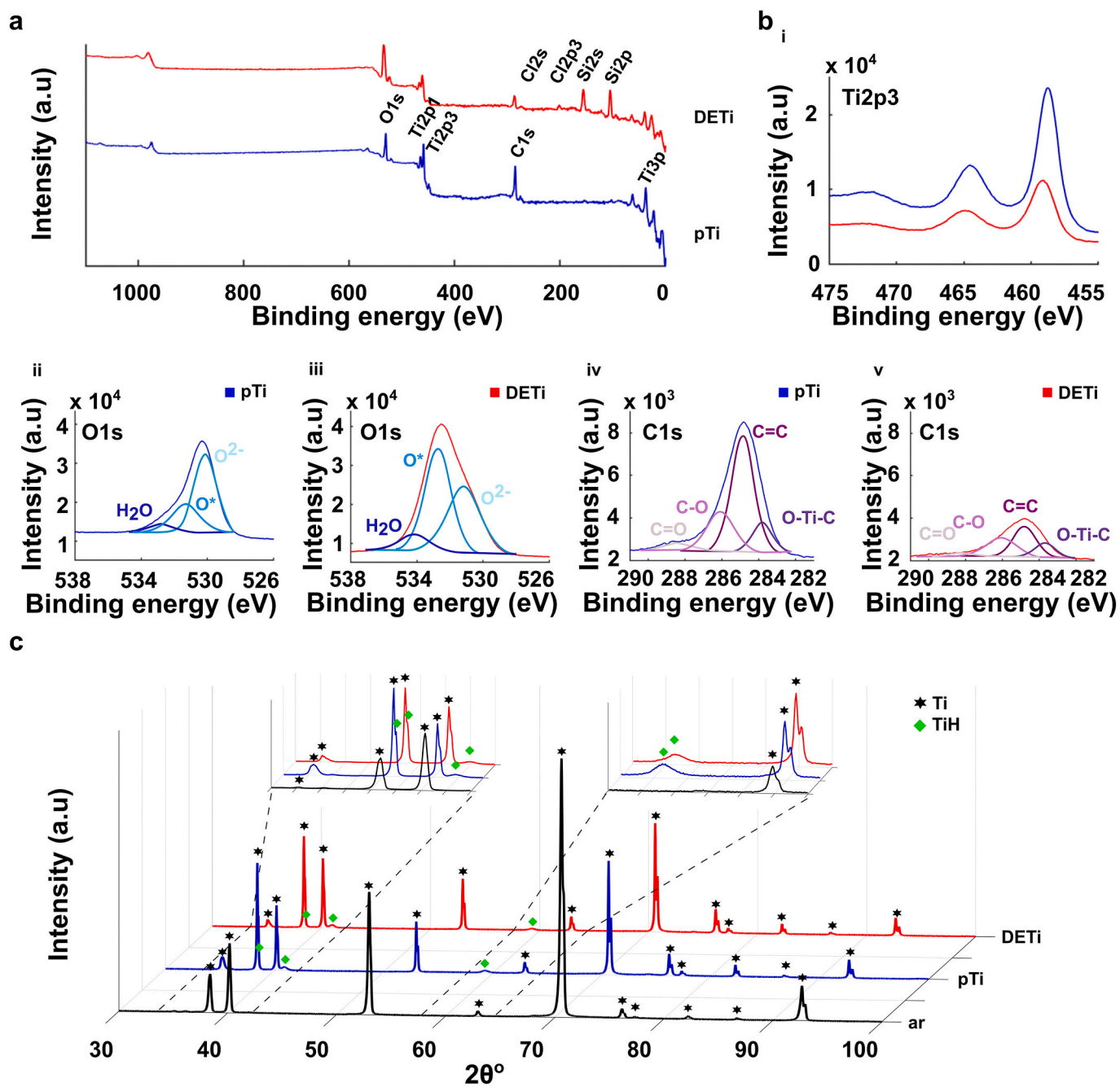


Fig. 4. a) XPS survey spectra of the polished titanium (pTi) and dry-etched titanium (DETi) samples; b) deconvolution of i) Ti2p₃ peak for pTi and DETi, ii) O1s peak for pTi, iii) O1s peak for DETi, iv) C1s peak for pTi, v) C1s for DETi; c) XRD patterns of as-received titanium (ar), pTi and DETi.

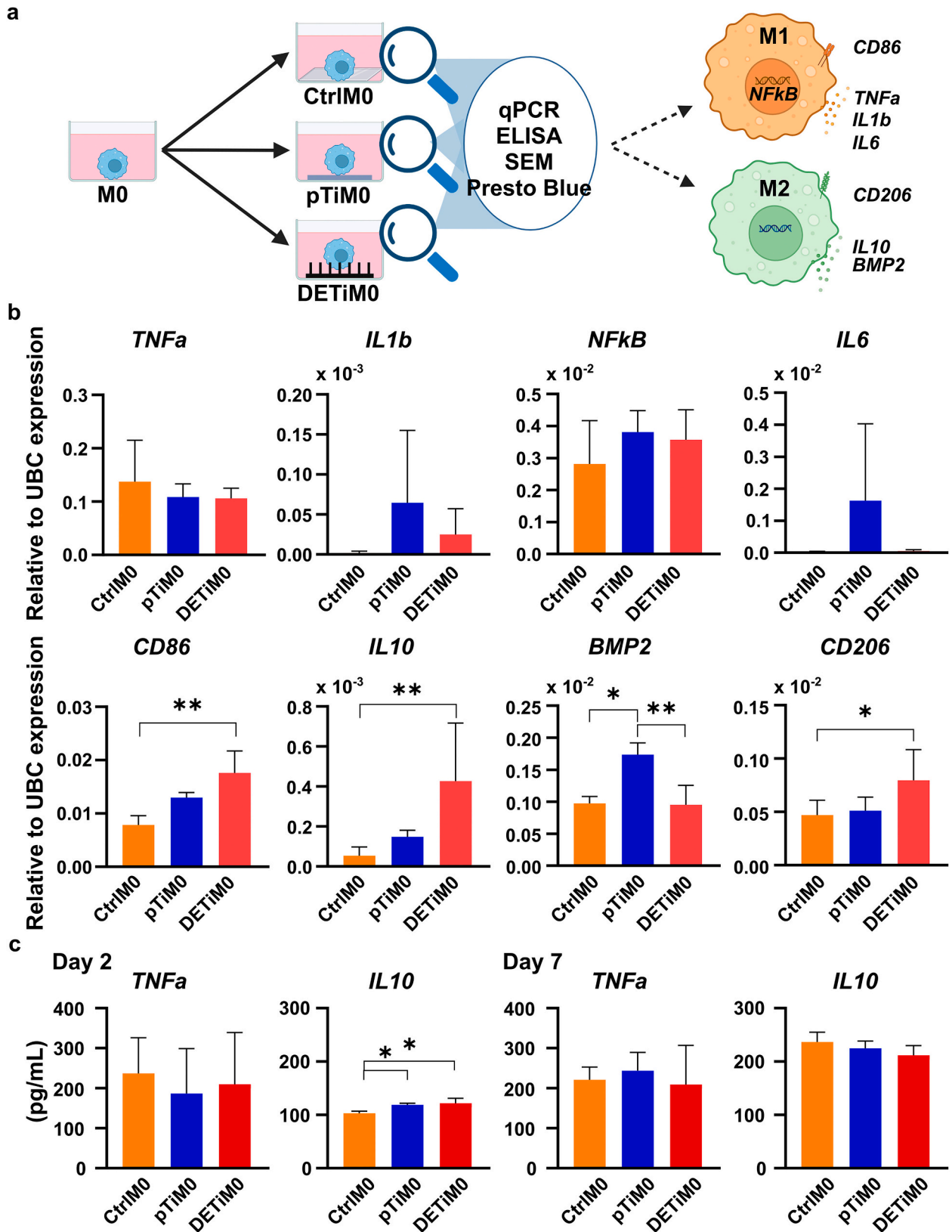


Fig. 5. a) Schematic overview of the experimental steps (biorender.com); b) pro- (*TNFα*, *IL1β*, *NFκB*, *IL6*, and *CD86*) and anti- (*IL10*, *BMP2*, *CD206*) inflammatory gene expression relative to the housekeeping gene (*UBC*) of unstimulated M0 macrophages on the glass control (CtrlM0), pTi (pTiM0) and DETi (DETiM0) surfaces after 48 h of culture. c) *TNFα* and *IL10* cytokine concentration in the culture medium of unstimulated M0 macrophages on the glass control (CtrlM0), pTi (pTiM0) and DETi (DETiM0) surfaces after 2 and 7 days of culture. **p* < 0.05, ***p* < 0.01, ****p* < 0.001.

The cross-sectional analyses by TEM showed a scalloped interface between the Ti substrate and the dry-etched region (Fig. 3a). The height of the pillars (PH) measured by TEM ranged from 730 nm to 2169 nm with an average of $PH = 1474 \pm 297$ nm, resulting in a pillar aspect ratio exceeding 9. Furthermore, the pillars revealed a different morphology along their height, with a dendritic network visible at the interface with the Ti substrate that developed into distinguishable bundled pillars towards the surface (Fig. 3a). The TEM-EDX elemental analysis clearly revealed the presence of Ti and O with traces of Al, Si, and Cl in the dry-etched layer relative to mostly Ti in the substrate (Fig. 3b, d, e). Interestingly, the TEM-SADP analyses (Fig. 3c) showed more crystalline phases detected in the upper regions towards the tip of the pillars and amorphous structures present in the dendritic area towards the interface with the Ti substrate. The crystalline structure detected in the clustered peaks consisted of crystals with lattice spacing of 2.11 Å, 1.81 Å, and 1.28 Å.

The surface chemistry analysis by XPS confirmed the dominant presence of Ti and O on the surfaces (Fig. 4a). In addition, in the polished sample, the majority of oxygen was found in the form of lattice oxygen species (O^{2-}) within TiO_2 (Fig. 4b ii) [21]. The remaining oxygen components consisted of oxygen vacancies (O^*) or surface-absorbed OH-groups and absorbed water (H_2O), attributed to contamination [22]. Carbon contamination was also noted (Fig. 4a, b iv, v). Following reactive ion etching, the oxygen vacancies increased, and the lattice oxides decreased (Fig. 4b iii). In contrast with the TEM-SADP analysis, the XRD findings revealed no differences in the crystalline titanium phases between pTi and DETi surfaces, showing no presence of TiO_2 crystalline structures on the DETi surfaces (Fig. 4c). However, the TiH phase was detected on the pTi and DETi samples but not on the as-received (ar) Ti samples.

3.2. Effects of the Ti substrates on unstimulated macrophages (M0)

Unstimulated M0 cells were seeded on the glass, pTi and DETi substrates to evaluate the effects of the surfaces on cells morphology and polarization (Fig. 5a). After 48 h of culture, the M0 cells expressed both pro- and anti-inflammatory genes on the glass, pTi and DETi substrates (Fig. 5b). No significant differences in the expression of pro-inflammatory genes were induced by the DETi and the pTi substrates relative to the glass control samples except for the *CD86* cell surface receptor, which was significantly upregulated on DETi compared to the glass control (Fig. 5b). By comparison, the DETi substrates upregulated two out of three anti-inflammatory genes relative to the controls, namely the *IL10* and *CD206* (Fig. 5b). For the pTi substrates only the *BMP2* gene was significantly upregulated relative to the control. No significant differences were found after 4 and 24 h (Figs. S1–S2). Cytokine secretion of M0 cells after 2 days showed significant increases in *IL10* synthesis for both titanium surfaces, and no differences were observed in *TNF α* concentration (Fig. 5c). The long-term effect of all the surfaces on M0 cells after 7 days showed no significant differences (Fig. 5c). These findings suggest that after 48 h of culture, the DETi substrates supported the polarization of M0 macrophages towards M1 and M2 phenotypes.

Morphological analysis of M0 macrophages by SEM revealed a difference between the cells interfaced with pTi and DETi (Figs. 6a–c, S5a). The macrophages on pTi were relatively round, developed numerous and long cellular protrusions in all directions, and had a rough surface, especially at longer culture time (24 and 48 h). The cells on DETi were more elongated, with shorter protrusions anchoring on the pillars and with a relatively smooth surface. Both substrates supported cell growth, and after 48 h of culture, the metabolic activity of the cells on DETi was significantly higher than on the pTi (Fig. 6d).

3.3. Effects of the Ti substrates on M1 stimulated macrophages

M1 stimulated cells were also seeded on the two Ti substrates to

simulate the pro-inflammatory microenvironment generated following implantation (Fig. 7a). Interestingly, after 48 h of culture, the pro-inflammatory markers analysed were still expressed by the M1 cells on both titanium substrates with *IL1b*, *IL6*, and *CD86* expression notably higher compared to the controls (Fig. 7b). Although the M1 cells showed higher expressions of *IL10* and *BMP2* M2 markers on the titanium substrates relative to the control, these differences were not significant, except for the *BMP2* gene on the pTi. Protein concentration, as measured by ELISA, did not show any differences between surfaces after two days of culture (Fig. 7c). However, the long-term effect showed a significantly lower *IL10* concentration in the DETi supernatant compared to the other two surfaces (Fig. 7c). The findings suggest a stronger pro-inflammatory response of M1 cells to both titanium substrates relative to the controls after two days, and a lower anti-inflammatory response after seven days on the DETi surface.

For M1 macrophages, morphological analysis by SEM revealed a comparable trend with the M0 cells (Figs. 8a–c, S5b). The M1 cells spread well on pTi after 4 h and became increasingly smaller and rougher after 24 and 48 h. On DETi surfaces, the M1 cells were more elongated, especially after 24 and 48 h (AR after 48 h = 2.13 ± 1.17 on DETi vs 1.68 ± 0.73 on pTi), smoother and maintained their area around $500 \mu m^2$ over the entire period. On both substrates, the M1 cells developed protrusions, but these were longer and more numerous on pTi than on DETi. As with M0 cells, the metabolic activity of the M1 cells increased significantly after 48 h (Fig. 8d).

Cross-sectional analyses by FIB-SEM showed that the cells could settle on top of the pillars (Fig. 8e) with some instances in which the cells seem to sink and engulf some of the clustered pillars locally. It is noteworthy to mention, however, that ion milling led to partial *in situ* destruction of the cell and underlying pillars, introducing uncertainty regarding the actual occurrence of this phenomenon and the precise point of separation between the surface and macrophage.

4. Discussion

The multifunctional properties of HAR nanostructured surfaces remain an interesting research area in terms of cell-instructive biomaterials. Previous studies have already shown that dry-etched titanium nanopillars fabricated by ICP-RIE under specific conditions can have both bactericidal and osteogenic properties [3–5,8,9]. The activation of mechanotransduction pathway involving focal adhesion kinase (FAK) and Rho-associated protein kinase (ROCK) was contributing to the improved osteogenic properties of these surfaces [10].

Nevertheless, the influence of such nanotopographies on immune cells has not been studied until now. It is known that both physical and biochemical stimuli can also activate the intracellular signaling pathways of macrophages, possibly leading to an improved antibacterial, followed by a pro-healing response [23,24].

Our study revealed new insights into the DETi pillars' characteristics by using TEM analyses that showed for the first time the presence of a dendritic network at the base of the pillars and a change in crystallinity along pillar height. In addition, the changes induced by the DETi surfaces on the morphology of J774A.1 murine macrophages and their polarization behavior pointed towards the immunomodulatory potential of these surfaces that can be harnessed not only for maximizing osteogenesis but also for enhancing their already proven antibacterial function.

The TEM-SADP images of the DETi cross-sections showed that the very top region of the pillars formed by the ICP-RIE process, consisted of crystalline TiO_2 , whereas the inner region exhibited a dendritic nanowire network of amorphous TiO_2 that merged with the crystalline Ti substrate. The formation of the crystalline TiO_2 phases was not evidenced by the XRD analysis most probably due to the larger penetration depth of the X-rays exceeding the etched surface and reaching the metallic substrate [6]. Nevertheless, the XRD results indicated some differences between the as-received Ti wafer (ar), and pTi and DETi

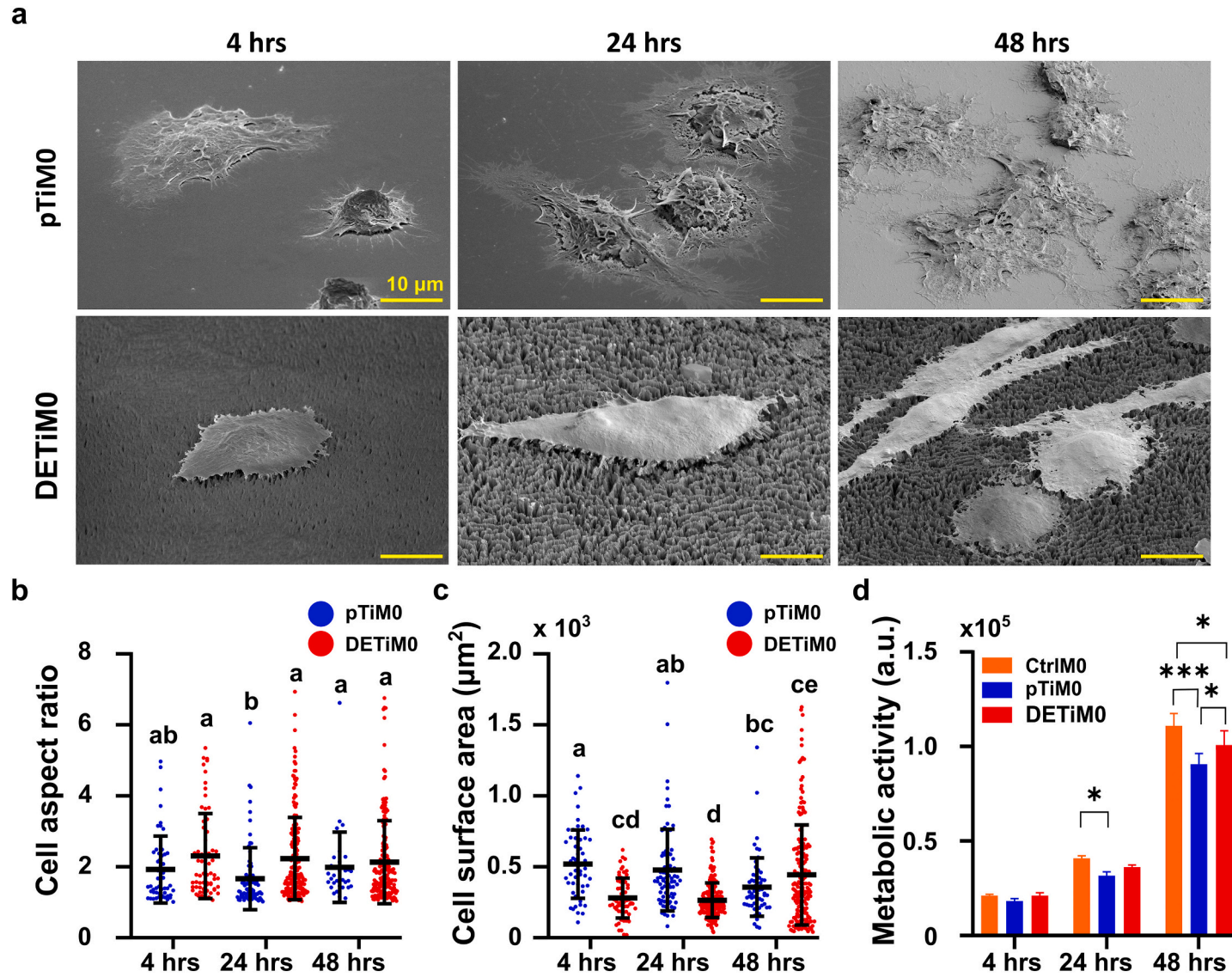


Fig. 6. a) SEM images of unstimulated M0 cells after 4, 24 and 48 h of culture on pTi and DETi; b) cell aspect ratio and c) mean cell surface area of M0 cells on pTi and DETi surfaces over time. At least 50 cells were studied per condition; groups with the same letters are not significantly different; d) metabolic activity of M0 macrophages on glass (CtrlM0), pTi and DETi. * $p < 0.05$, ** $p < 0.01$, *** $p < 0.001$.

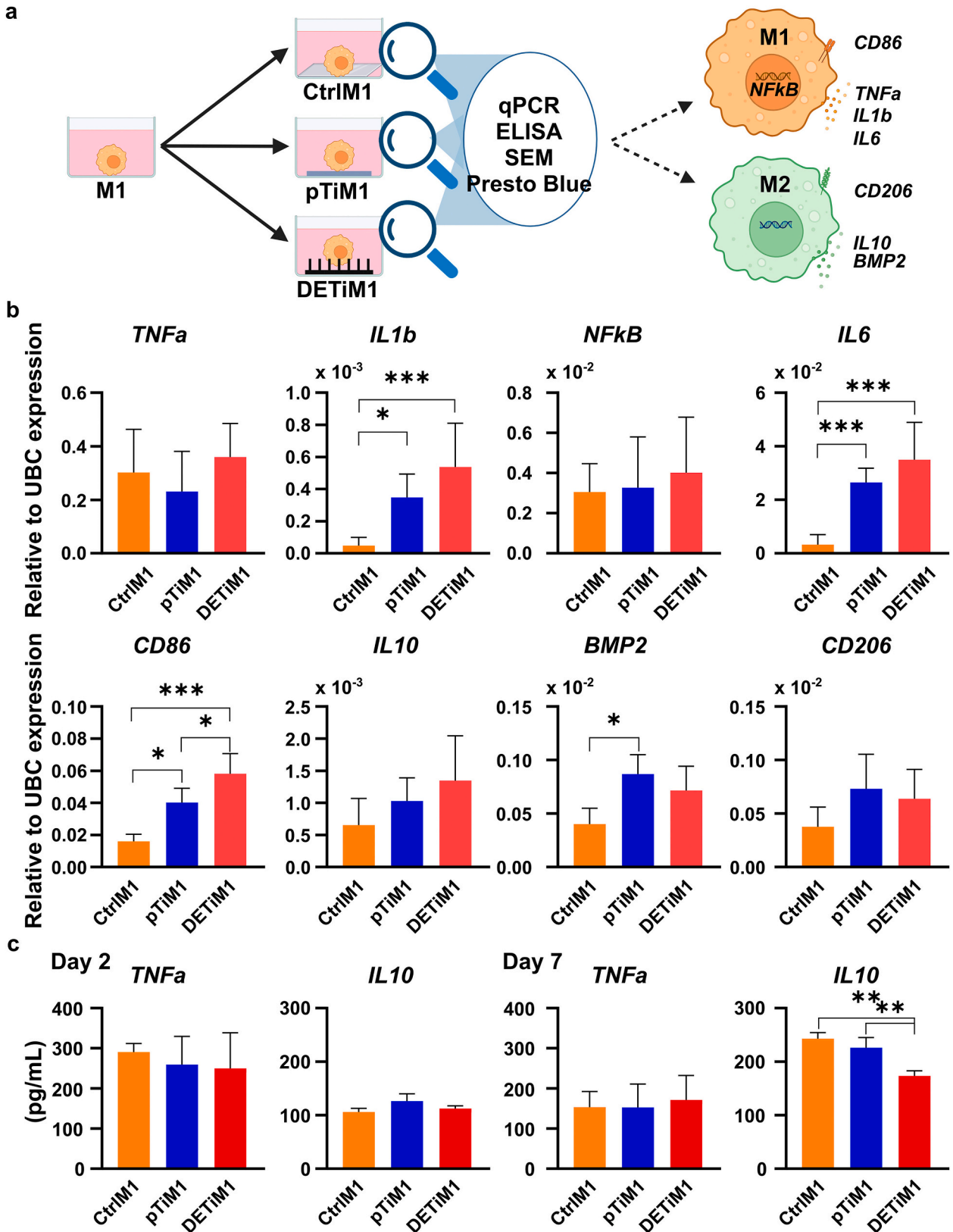


Fig. 7. a) Schematic overview of the experimental steps (biorender.com); b) pro- (*TNFα*, *IL1β*, *NfκB*, *IL6*, and *CD86*) and anti- (*IL10*, *BMP2*, *CD206*) inflammatory gene expression relative to the housekeeping gene (*UBC*) of M1 stimulated macrophages on the glass control (CtrlM1), DETi (DETiM1) and pTi (pTiM1) surfaces after 48 h of culture. c) *TNFα* and *IL10* cytokine concentration in the culture medium of M1 stimulated macrophages on the glass control (CtrlM1), pTi (pTiM1) and DETi (DETiM1) surfaces after 2 and 7 days of culture. * $p < 0.05$, ** $p < 0.01$, *** $p < 0.001$.

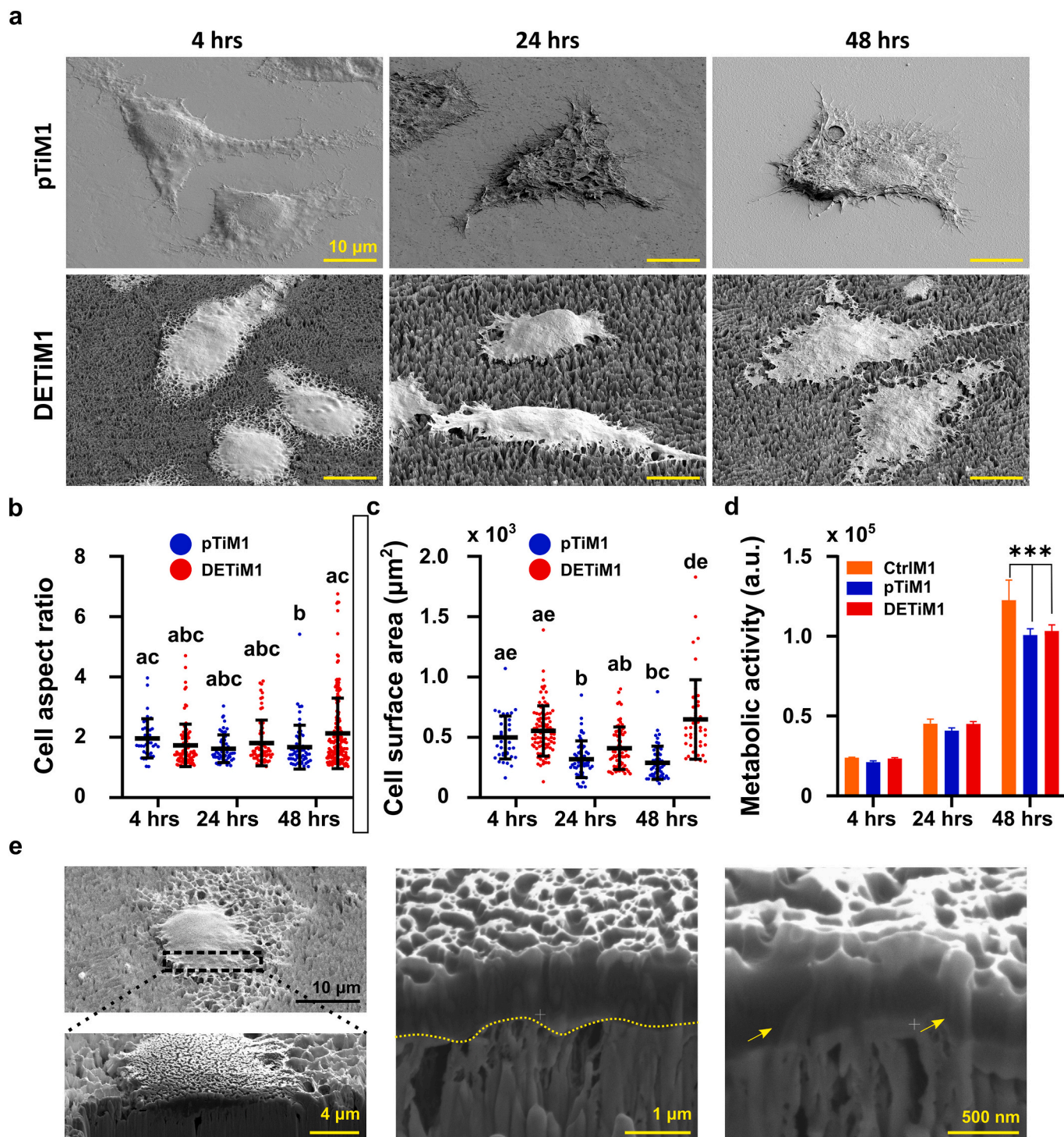


Fig. 8. a) SEM images of M1 stimulated cells after 4, 24 and 48 h of culture on pTi and DETi; b) cell aspect ratio and c) mean cell surface area of cells on pTi and DETi surfaces over time. At least 50 cells were studied per condition; groups with the same letters are not significantly different; d) metabolic activity of M1 macrophages on glass (CtrlM1), pTi and DETi measured using Presto Blue assay. * $p < 0.05$, ** $p < 0.01$, *** $p < 0.001$. e) Focused ion beam–scanning electron microscopy (FIB-SEM) cross-sectional images of M1 cells after 24 h of culture on DETi at different magnifications. Yellow arrows indicate possible cellular penetration by nanopillars.

samples (Fig. 4c). The peaks identifying TiH crystalline structures on the pTi surfaces and not on the as-received wafers suggest that the CMP polishing introduced H contamination on the surface. The CMP method was conducted with silicate slurry containing 74 % dH₂O and < 1 % KOH. Although KOH normally protects titanium from hydrogen uptake, extreme conditions such as the mechanical forces applied to the surface could have allowed this minimal TiH contamination [25]. However, since the peak was very small and such a phase was not found by the cross-section TEM-SADP measurements, no direct effects on the formation of the nanopillars are expected.

The origins of the dendritic nanowire network of amorphous TiO₂ may originate from the argon ion bombardments, which form point defects in TiO₂ crystalline structures by displacing oxygen atoms from their respective equilibrium positions and thus introducing oxygen vacancies [26]. Such oxygen vacancies were confirmed in our study via XPS analysis (Fig. 4b ii–iii) and also found in other studies after the dry-etching process of titanium [2,6,7] suggesting that also in the development of DETi, point defects are introduced in the resulting TiO₂ layer. These vacancies are essential for promoting the chemical reaction between Cl and Ti, and thus enhancing the dry etching efficiency of Ti [27]. However, a side effect of this increase in point defects, is the increase in lattice destabilization of the crystalline TiO₂ surface, which results in the amorphous nature of the dendritic nanowire network [26].

In addition to the previous studies on the osteogenic and bactericidal biofunctionalities of dry-etched titanium surfaces [2,8,9], this study reveals the effects of these surfaces on macrophages, cells that can actually mediate both of the above biofunctionalities post-implantation.

The cells could attach to both titanium substrates. However, the two different substrates induced different morphological characteristics in the cells. Both the M0 and M1 cells showed a more elongated shape, a smoother surface, and shorter cellular protrusions on the DETi compared to the pTi. This could be the combined effect of the specific topography of the DETi and associated hydrophilicity compared to the pTi surfaces. The hydrophilic DETi surfaces support cell spreading, but the presence of subcellular scale pillars, ridges and pores may impede cell migration, favoring their elongation and formation of shorter cellular protrusions anchoring on the nearby pillars. The ruffle cell membrane observed on the pTi surfaces may indicate an enhanced macropinocytosis function of these cells compared to the cells on DETi [28].

The M0 cells expressed both M1 and M2 markers on DETi indicating the presence of both phenotypes after 48 h of culture. Protein analyses by ELISA confirmed a more dominant M2 presence by the higher *IL10* concentration in the supernatant from titanium surfaces. This suggests a shift of M0 cells towards M2 phenotype after 48 h of culture. The M1 cells also expressed M1 and M2 markers on DETi but these cells showed a stronger pro-inflammatory response on DETi compared to the glass controls. More specifically, the DETi surfaces upregulated the levels of *CD86*, *IL10* and *CD206* for M0 cells and *IL1b*, *IL6* and *CD86* for M1 cells after 48 h.

Although we have shown that after seven days of culture, the anti-inflammatory response of M1 stimulated macrophages is lower on DETi surfaces, we believe that the dynamics of the immunomodulatory effects of such surfaces deserves further attention by using osteoimmunology co-culture models that may reveal the full potential of such surfaces. Co-culture with osteogenic cells is essential as it would capture the cell-cell communication taking place between these cells during tissue regeneration. It is already known that in co-cultures, a short *TNFa* burst followed by *IL10* secretion improves the anti-inflammatory response, and the pro-healing effects of MSCs [29]. On top of that, it has already been found that preosteoblasts thrive on these HAR surfaces [2,8,9], and therefore, the resulting crosstalk holds the potential for controlling the initial pro-inflammatory response of M1 stimulated macrophages, which

is essential for both bone regeneration and bacterial eradication [18]. Furthermore, *IL1b* enhances macrophage phagocytosis and an increase of *IL1b*, and *IL6* in combination with *IL10* could indicate a M2b phenotype [30]. This was the case of M1 on DETi surfaces (Fig. 7b). This phenotype is generally related to being anti-inflammatory, helps in the activation of Th2 helper cells, and introduces bone healing. Together with the previously evidenced bactericidal effects of the DETi [2,8,9], these surfaces may show osteogenic, immunomodulatory and antibacterial biofunctionalities.

Towards this aim, the development of carefully designed bacterial-mammalian cell co-culture models becomes crucial. These models should consider a sufficient bacterial load to mimic *in vivo* infections and provide a favorable environment for macrophages/osteoprogenitors survival [31].

Furthermore, combining these subcellular topographies with optimum geometries at the scaffold scale, including controlled pore shapes and surface curvatures, will further help in enhancing the regenerative properties of the scaffolds. Apart from their bactericidal nature, using HAR pillars as a surface treatment may generate subcellular topographical cues that can be sensed by the cells and influence their attachment and migration. Furthermore, the high density of the pillars and the hydrophilic properties of the DETi surfaces support cell spreading and increase cytoskeletal tension with beneficial effects on osteogenesis and osseointegration. [4,32]. Microbial infections and unsatisfactory osseointegration remain the most encountered causes of bone implant failure to date [33]. Proper surface modification such as the introduction of HAR pillars could prevent this in the future. To this aim, the effects of Ti ICP-RIE HAR pillars on the immune cells need to be unravelled, as these can strongly influence both the osteogenic and bactericidal potential of such surfaces. We believe that such studies should be part of the biocompatibility evaluation in the future for biomaterials intended to stimulate tissue repair/regeneration, as the inflammation phase precedes the tissue repair phase, and the biomaterials may also induce beneficial immunomodulatory effects. With our study, we have taken an important step forward in the development of titanium surfaces that can have osteogenic, bactericidal and immunomodulatory properties for bone implants. The short-term immunomodulatory results look promising, although the negative effect on the anti-inflammatory response after seven days requires more research to optimise the immunomodulatory function of these surfaces. The aforementioned co-culture models could unravel the effect of this inflammatory response on the bactericidal and osteogenic effect. In parallel, multiple strategies are explored for the development of antibacterial orthopedic biomaterials that can overcome AMR, from the usage of silver ion-based biomaterials [34] to drug delivery systems for on-demand delivery of antibacterial peptide from implant surfaces [35]. Eventually, through single or integrated approaches based on physical and/or chemical cues, regenerative biomaterials for future bone implants endowed with the needed multiple biofunctionalities will be developed.

5. Conclusion

The immunomodulatory biofunctionality of biomaterials is increasingly recognized as a biocompatibility requirement for bone implants. This study explored the effects of titanium high-aspect ratio nanopillars produced by dry-etching on the morphology and polarization of M0 unstimulated and M1 stimulated macrophages. The physicochemical characterization by TEM revealed changes in morphology and crystallinity along the height of the pillars. Both the M0 and M1 cells could attach and spread on the dry-etched surfaces adopting an elongated shape as a result of the hydrophilicity, roughness and specific topography of such surfaces. In addition, the M0 cells on DETi polarized to M1

and M2 phenotypes whereas M1 cells showed M2-like morphologies but a stronger pro-inflammatory response relative to the glass controls. The findings of this study reveal for the first time the immunomodulatory potential of such surfaces that should be further explored in co-culture models involving skeletal and/or bacterial cells for the development of regenerative biomaterials with integrated osteogenic, immunomodulatory, and antibacterial properties for bone implants.

CRedit authorship contribution statement

Benedictus I.M. Eijkel: Writing – review & editing, Writing – original draft, Visualization, Validation, Methodology, Investigation, Formal analysis, Data curation, Conceptualization. **Khashayar Modaresifar:** Writing – review & editing, Methodology, Investigation. **Eszter Mádai:** Writing – review & editing, Validation, Investigation, Formal analysis. **Mahya Ganjian:** Writing – review & editing, Methodology, Investigation. **Peyman Taheri:** Resources. **Iulian Apachitei:** Writing – review & editing, Supervision, Resources, Project administration, Funding acquisition. **Lidy E. Fratila-Apachitei:** Writing – review & editing, Writing – original draft, Validation, Supervision, Resources, Methodology, Conceptualization.

Declaration of competing interest

The authors declare no conflict of interest.

Acknowledgments

This publication is part of the project DARTBAC (with project number NWA.1292.19.354) of the research programme NWA-ORC which is (partly) financed by the Dutch Research Council (NWO). For the TEM results, we acknowledge support from the Kavli Institute of Nanoscience, Delft University of Technology, and the Netherlands Electron Microscopy Infrastructure (NEMI), project number 184.034.014, part of the National Roadmap and financed by the Dutch Research Council (NWO). The XRD analyses were performed by Ruud Hendriks at the Department of Materials Science and Engineering of the Delft University of Technology.

Appendix A. Supplementary data

Supplementary data to this article can be found online at <https://doi.org/10.1016/j.bioadv.2025.214321>.

Data availability

Data will be made available on request.

References

- X. Liu, P. Chu, C. Ding, Surface modification of titanium, titanium alloys, and related materials for biomedical applications, *Mater. Sci. Eng. R. Rep.* 47 (2004) 49–121, <https://doi.org/10.1016/j.mser.2004.11.001>.
- J. Hasan, S. Jain, K. Chatterjee, Nanoscale topography on black titanium imparts multi-biofunctional properties for orthopedic applications, *Sci. Rep.* 7 (2017) 41118, <https://doi.org/10.1038/srep41118>.
- K. Modaresifar, S. Azizian, M. Ganjian, L.E. Fratila-Apachitei, A.A. Zadpoor, Bactericidal effects of nanopatterns: a systematic review, *Acta Biomater.* 83 (2019) 29–36, <https://doi.org/10.1016/j.actbio.2018.09.059>.
- S.G. Higgins, M. Bece, A. Belessiotis-Richards, H. Seong, J.E. Sero, M.M. Stevens, High-aspect-ratio nanostructured surfaces as biological metamaterials, *Adv. Mater.* 32 (2020) 1903862, <https://doi.org/10.1002/adma.201903862>.
- J. Jenkins, J. Mantell, C. Neal, A. Gholinia, P. Verkade, A.H. Nobbs, B. Su, Antibacterial effects of nanopillar surfaces are mediated by cell impedance, penetration and induction of oxidative stress, *Nat. Commun.* 11 (11) (2020) 1–14, <https://doi.org/10.1038/s41467-020-15471-x>.
- D.P. Linklater, S. Juodkazis, R.J. Crawford, E.P. Ivanova, Mechanical inactivation of *Staphylococcus aureus* and *Pseudomonas aeruginosa* by titanium substrata with hierarchical surface structures, *Materialia* 5 (2019), <https://doi.org/10.1016/j.MTLA.2018.100197>.
- A. Roy, S.K. Gupta, S. Suwas, K. Chatterjee, The significance of crystallographic texture in dry etching of titanium to engineer bioinspired nanostructured bactericidal surfaces, *JOM* 74 (2022) 3367–3378, <https://doi.org/10.1007/s11837-022-05395-w>.
- V. Martel-Frchet, E.P. Ivanova, T. Le Clainche, D. Linklater, S. Wong, P. Le, S. Juodkazis, X. Le Guevel, J.L. Coll, Mechano-bactericidal titanium surfaces for bone tissue engineering, *ACS Appl. Mater. Interfaces* 12 (2020) 48272–48283, <https://doi.org/10.1021/ACSAMI.0C11502>.
- K. Modaresifar, M. Ganjian, L. Angeloni, M. Minneboo, M.K. Ghatkesar, P. Hagedoorn, L.E. Fratila-Apachitei, A.A. Zadpoor, On the use of black Ti as a bone substituting biomaterial: behind the scenes of dual-functionality, *Small* 17 (2021) 2100706, <https://doi.org/10.1002/smll.202100706>.
- K. Modaresifar, M. Ganjian, P.J. Diaz-Payno, M. Klimopoulou, M. Koedam, B.C. J. van der Eerden, L.E. Fratila-Apachitei, A.A. Zadpoor, Mechanotransduction in high aspect ratio nanostructured meta-biomaterials: the role of cell adhesion, contractility, and transcriptional factors, *Mater. Today Bio* 16 (2022) 100448, <https://doi.org/10.1016/j.mtbio.2022.100448>.
- A. Jaggessar, A. Mathew, H. Wang, T. Tesfamichael, C. Yan, P.K. Yarlagadda, Mechanical, bactericidal and osteogenic behaviours of hydrothermally synthesised TiO₂ nanowire arrays, *J. Mech. Behav. Biomed. Mater.* 80 (2018) 311–319, <https://doi.org/10.1016/j.jmbbm.2018.02.011>.
- T. Diu, N. Faruqui, T. Sjöström, B. Lamarre, H.F. Jenkinson, B. Su, M.G. Ryadnov, Cicada-inspired cell-instructive nanopatterned arrays, *Sci. Rep.* 4 (2014) 7122, <https://doi.org/10.1038/srep07122>.
- R. Bright, D. Fernandes, J. Wood, D. Palms, A. Burzava, N. Ninan, T. Brown, D. Barker, K. Vasilev, Long-term antibacterial properties of a nanostructured titanium alloy surface: an in vitro study, *Mater. Today Bio* 13 (2022), <https://doi.org/10.1016/j.mtbio.2021.100176>.
- M. Ganjian, K. Modaresifar, H. Zhang, P.L. Hagedoorn, L.E. Fratila-Apachitei, A. A. Zadpoor, Reactive ion etching for fabrication of biofunctional titanium nanostructures, *Sci. Rep.* 9 (2019), <https://doi.org/10.1038/s41598-019-55093-y>.
- A. Roy, K. Chatterjee, Bactericidal anisotropic nanostructures on titanium fabricated by maskless dry etching, *ACS Appl. Nano Mater.* 5 (2022) 4447–4461, <https://doi.org/10.1021/acsnan.2c00555>.
- D.P. Linklater, H.K.D. Nguyen, C.M. Bhadra, S. Juodkazis, E.P. Ivanova, Influence of nanoscale topology on the bactericidal efficiency of black silicon surfaces, *Nanotechnology* 28 (2017) 469501, <https://doi.org/10.1088/1361-6528/aa8ce6>.
- E.P. Ivanova, J. Hasan, H.K. Webb, G. Gervinskis, S. Juodkazis, V.K. Truong, A.H. F. Wu, R.N. Lamb, V.A. Baulin, G.S. Watson, J.A. Watson, D.E. Mainwaring, R. J. Crawford, Bactericidal activity of black silicon, *Nat. Commun.* 4 (1) (2013) 1–7, <https://doi.org/10.1038/ncomms3838>.
- G. Mestres, S.-S.D. Carter, N.P. Hailer, A. Diez-Escudero, A practical guide for evaluating the osteoimmunomodulatory properties of biomaterials, *Acta Biomater.* 130 (2021) 115–137, <https://doi.org/10.1016/j.actbio.2021.05.038>.
- Z. Chen, T. Klein, R.Z. Murray, R. Crawford, J. Chang, C. Wu, Y. Xiao, Osteoimmunomodulation for the development of advanced bone biomaterials, *Mater. Today* 19 (2016) 304–321, <https://doi.org/10.1016/j.matod.2015.11.004>.
- J. Dong, W. Wang, W. Zhou, S. Zhang, M. Li, N. Li, G. Pan, X. Zhang, J. Bai, C. Zhu, Immunomodulatory biomaterials for implant-associated infections: from conventional to advanced therapeutic strategies, *Biomater. Res.* 26 (2022), <https://doi.org/10.1186/S40824-022-00326-X>.
- L.P. Delgado, M.Z. Figueroa-Torres, M.C. Ceballos-Chuc, R. García-Rodríguez, J. J. Alvarado-Gil, G. Oskam, G. Rodríguez-Gattorno, Tailoring the TiO₂ phases through microwave-assisted hydrothermal synthesis: comparative assessment of bactericidal activity, *Mater. Sci. Eng. C* 117 (2020), <https://doi.org/10.1016/j.msec.2020.111290>.
- V. Singh, A. Rao, A. Tiwari, P. Yashwanth, M. Lal, U. Dubey, S. Aich, B. Roy, Study on the effects of Cl and F doping in TiO₂ powder synthesized by a sol-gel route for biomedical applications, *J. Phys. Chem. Solids* 134 (2019) 262–272, <https://doi.org/10.1016/j.jpcs.2019.06.011>.
- J. Kim, Y.J. Shin, L.J. Ha, D. Kim, D. Kim, Unraveling the mechanobiology of the immune system, *Adv. Healthc. Mater.* 8 (2019), <https://doi.org/10.1002/adhm.201801332>.
- G.R. Pidwill, J.F. Gibson, J. Cole, S.A. Renshaw, S.J. Foster, The role of macrophages in *Staphylococcus aureus* infection, *Front. Immunol.* 11 (2021) 620339, <https://doi.org/10.3389/fimmu.2020.620339>.
- Y. Zhu, T. Wook Heo, J.N. Rodriguez, P.K. Weber, R. Shi, B.J. Baer, F.F. Morgado, S. Antonov, K.E. Kweon, E.B. Watkins, D.J. Savage, J.E. Chapman, N.D. Keilbart, Y. Song, Q. Zhen, B. Gault, S.C. Vogel, S.T. Sen-Britain, M.G. Shalloo, C. Orme, M. Bagge-Hansen, C. Hahn, T.A. Pham, D.D. Macdonald, S. Roger Qiu, B.C. Wood, Hydriding of titanium: recent trends and perspectives in advanced characterization and multiscale modeling, *Curr. Opin. Solid State Mater. Sci.* 26 (2022) 101020, <https://doi.org/10.1016/j.cossms.2022.101020>.
- K. Piler, C. Bahrim, S. Twagirayezu, T.J. Benson, Lattice disorders of TiO₂ and their significance in the photocatalytic conversion of CO₂, in: *Adv. Catal. Academic Press Inc.*, 2020, pp. 109–233, <https://doi.org/10.1016/bs.acat.2020.09.001>.
- F. Fracassi, R. d'Agostino, Chemistry of titanium dry etching in fluorinated and chlorinated gases, *Pure Appl. Chem.* 64 (1992) 703–707, <https://doi.org/10.1351/pac199264050703>.
- S.E. Quinn, L. Huang, J.G. Kerkvliet, J.A. Swanson, S. Smith, A.D. Hoppe, R. B. Anderson, N.W. Thiex, B.L. Scott, The structural dynamics of macropinosome formation and PI3-kinase-mediated sealing revealed by lattice light sheet microscopy, *Nat. Commun.* 12 (2021) 4838, <https://doi.org/10.1038/s41467-021-25187-1>.

- [29] F. Loi, L.A. Cordova, J. Pajarinen, T.H. Lin, Z.Y. Yao, S.B. Goodman, Inflammation, fracture and bone repair, *Bone* 86 (2016) 119–130, <https://doi.org/10.1016/j.bone.2016.02.020>.
- [30] L. xun Wang, S. xi Zhang, H. juan Wu, X. lu Rong, J. Guo, M2b macrophage polarization and its roles in diseases, *J. Leukoc. Biol.* 106 (2019) 345–358, <https://doi.org/10.1002/JLB.3RU1018-378RR>.
- [31] B.I.M. Eijkel, I. Apachitei, L.E. Fratila-Apachitei, A.A. Zadpoor, In vitro co-culture models for the assessment of orthopedic antibacterial biomaterials, *Front. Bioeng. Biotechnol.* 12 (2024) 1332771, <https://doi.org/10.3389/FBIOE.2024.1332771/BIBTEX>.
- [32] H. Donnelly, M.J. Dalby, M. Salmeron-Sanchez, P.E. Sweeten, Current approaches for modulation of the nanoscale interface in the regulation of cell behavior, *Nanomedicine* 14 (7) (2018) 2455–2464, <https://doi.org/10.1016/j.nano.2017.03.020>.
- [33] Y. Bian, T. Hu, Z. Lv, Y. Xu, Y. Wang, H. Wang, W. Zhu, B. Feng, R. Liang, C. Tan, X. Weng, Bone tissue engineering for treating osteonecrosis of the femoral head, *Exploration* 3 (2023) 20210105, <https://doi.org/10.1002/EXP.20210105>.
- [34] N.E. Putra, M.A. Leeflang, V. Ducret, V. Patrula, L.E. Fratila-Apachitei, K. Perron, H. Ye, J. Zhou, I. Apachitei, A.A. Zadpoor, Preventing antibiotic-resistant infections: additively manufactured porous Ti6Al4V biofunctionalized with Ag and Fe nanoparticles, *Int. J. Mol. Sci.* 23 (2022) 13239, <https://doi.org/10.3390/ijms232113239>.
- [35] M. Šalandová, M.A. Leeflang, M. Klimopoulou, L.E. Fratila-Apachitei, I. Apachitei, A.A. Zadpoor, On-demand magnetically-activated drug delivery from additively manufactured porous bone implants to tackle antibiotic-resistant infections, *Adv. Mater. Technol.* 9 (2024) 2301616, <https://doi.org/10.1002/admt.202301616>.